JOURNAL OF GEOPHYSICAL RESEARCH, VOL. 112, B09102, doi:10.1029/2007JB004961, 2007

Click Here for Full Article

Stochastic analysis of exit fluid temperature records from the active TAG hydrothermal mound (Mid-Atlantic Ridge, 26°N): 2. Hidden Markov models of flow episodes

R. A. Sohn[1]

Received 30 January 2007; revised 15 May 2007; accepted 1 June 2007; published 12 September 2007.

[1] I develop a stochastic signal model for episodic modes of variability in hydrothermal flow records using probabilistic functions of Markov processes (i.e., hidden Markov models, HMMs) and fit the model to exit fluid temperature time series data from diffuse flow sites on the active TAG hydrothermal mound. The flow states are modeled using Gamma densities to provide flexibility for application to a range of signal types. Between three and five flow states are needed to fit the diffuse flow temperature records from TAG, which correspond to models with between 10 and 28 degrees of freedom. The number of flow states required to fit a given record is related to the signal variance, with more variable records requiring a larger state space. HMMs thus provide an efficient signal model for episodic variability in hydrothermal flow records, suggesting that Markov processes may provide a means to generate stochastic subsurface flow models for deep-sea hydrothermal fields if the spatial flow correlations can be incorporated into a statistical framework. I also use the Viterbi algorithm to "decode" the time series data into best fitting state sequences, which can be used to classify the records into discrete flow episodes. This may provide an objective means to identify discrete events in a flow record if misclassification issues arising from nonepisodic variability (e.g., tidal forcing) can be addressed.

Citation: Sohn, R. A. (2007), Stochastic analysis of exit fluid temperature records from the active TAG hydrothermal mound (Mid-Atlantic Ridge, 26°N): 2. Hidden Markov models of flow episodes, *J. Geophys. Res.*, *112*, B09102, doi:10.1029/2007JB004961.

1. Introduction

[2] Hydrothermal fluids at mid-ocean ridges (MORs) circulate within a dynamic subsurface medium that is continually perturbed by volcanic and tectonic processes, as well as the intrinsic processes of mineralization and hydrofracture. Geologic and hydrologic processes may impart rapid changes to the stress, permeability, and temperature fields of the subsurface circulation regime, and can thus generate episodic perturbations to the physical and chemical properties of hydrothermal exit fluids. These kinds of perturbations have been observed in a variety of hydrogeologic settings along the global MOR [e.g., *Davis et al.*, 2004; *Dziak et al.*, 2003; *Johnson et al.*, 2000; *Sohn et al.*, 1998], and the causal relationship between the flow perturbation and response can be exploited to advance our understanding of these complex and hard-to-observe hydrological systems.

[3] Much of the research to date has focused on developing physical models for the response of hydrothermal fluids to perturbation mechanisms in specific settings. *Wilcock* [2004] has developed models for the response of hydrothermal fluids to thermal and mechanical perturbations in volcanically active regions, and *Davis et al.* [2004] have modeled the pressure response of fluids to a tectonic earthquake swarm on a sedimented ridge. These physical models allow us to use geological flow perturbations to constrain hard-to-measure subsurface flow parameters, such as velocity, diffusivity, and permeability, which is vitally important for understanding the hydrogeology of deep-sea hydrothermal systems where logistical issues preclude the use of many standard perturbation techniques (e.g., pumping and tracer injection) employed in subaerial field areas.

[4] The general problem of modeling the flow response to extrinsic and intrinsic hydrogeological processes at MORs, however, remains poorly understood because we are critically lacking quantitative constraints regarding the influence of perturbation parameters on subsurface flow. For example, we do not yet understand how the size, position, and focal mechanism parameters of an earthquake influence the triggering, magnitude and timing of flow perturbations at a given site. Mid-ocean ridges are high-seismicity rate environments [e.g., *deMartin et al.*, 2007; *Wilcock et al.*, 2002], and without a basic understanding of these sensitivities it can be very difficult to associate flow perturbations with specific events. How can we tell, for example, if a given flow perturbation resulted from a large, distant earthquake, as opposed to a small, nearby event. The first-order sensitivity of hydrothermal flow to various kinds of

[1]Woods Hole Oceanographic Institution, Woods Hole, Massachusetts, USA.

Copyright 2007 by the American Geophysical Union.
0148-0227/07/2007JB004961$09.00

geological perturbations must be quantified before we can confidently use these episodes to model hydrothermal flow, and this can only be accomplished via statistical analysis of flow records and their correlation with accompanying event catalogues.

[5] Observations of hydrothermal exit fluid properties over statistically significant time intervals have recently become available for a few vent fields [e. g., *Larson et al.*, 2007; *Scheirer et al.*, 2006; *Sohn*, 2007], and these data exhibit a wide range of perturbation characteristics. The flow records generally cannot be explained with simple perturbation response models, and appear to require that flow properties are modulated by multiple subsurface processes operating over a range of temporal and spatial scales. The complicated nature of hydrothermal flow records acquired over multiyear time intervals motivates the development of stochastic models to quantify the statistical properties of episodic variability. Stochastic methods have proven effective for modeling complex subaerial hydrologic systems [e.g., *Rubin*, 2003, and references therein], and they can be used both to simulate flow and to estimate the statistical properties (e.g., mean and variance) of key subsurface flow parameters such as permeability and velocity. Stochastic (spectral) methods have been used to study periodic variability related to tidal forcing in hydrothermal exit fluid properties [e.g., *Little et al.*, 1988; *Tivey et al.*, 2002], but stochastic models for episodic variability associated with geologic perturbations have not been developed.

[6] In this paper I use probabilistic functions of Markov processes (i.e., hidden Markov models) to develop a stochastic signal model for episodic variability in deep-sea hydrothermal flow records. I use maximum likelihood methods to fit the signal model to diffuse exit fluid temperature records from the TAG active hydrothermal mound (26°N, Mid-Atlantic Ridge), and find that the flow records can be fit with HMMs employing between three and five states, which corresponds to 10 and 28 degrees of freedom, respectively. I consider the issues of model order and selection, and demonstrate how the Viterbi algorithm can be used to decode the time series into a best fitting state structure, from which an event history may be extracted. I conclude by considering the issue of using Markov processes to generate a synoptic stochastic flow model for a hydrothermal field, and identifying important topics for future research.

[7] This paper deals exclusively with statistical analyses of diffuse flow records from the active TAG mound. The implications of the temperature records for subsurface flow, and a discussion of the physical mechanisms generating exit fluid temperature variations, are covered in a companion manuscript [*Sohn*, 2007].

2. Hidden Markov Models of Hydrothermal Flow

[8] Hidden Markov models (HMMs) are probabilistic functions of Markov chains that provide a powerful analytical tool for modeling episodic time series data (for a general review, see *Ephraim* [2002]). The earliest research is due to Baum and colleagues, who applied HMMs to problems in population ecology [*Baum and Eagon*, 1967; *Baum and Petrie*, 1966], but perhaps the largest body of literature stems from applications in information and communications theory, where hidden Markov models are used for a variety of purposes, including automatic speech recognition [e.g., *Rabiner*, 1989, and references therein].

[9] In an HMM, each sample in a time series is associated with a state variable. The state variables cannot be directly observed, but rather must be deduced from the sample values (thus the use of the term, "hidden"). The time series, which is traditionally called the observation sequence, transitions between the unobservable states according to the probability rules of a Markov chain. Each state has its own unique probability density function, and the values of the observation sequence are drawn from the density function associated with the state in which the process resides at each time step. The state density functions are sufficiently distinct such that state transitions generate episodic behavior in the observation sequence.

[10] Statistical inference for HMMs usually focuses on estimating the state density functions, the probability rules governing state transitions, and the "hidden" state sequence. In some cases, including the present application, the number of states is not known a priori, and must also be estimated. A mathematical description of HMMs and the model fitting process for hydrothermal flow records is presented in the sections 2.1–2.4.

2.1. Probabilistic Functions of Markov Chains

[11] Consider a discrete time stochastic process that generates a sequence of random variables $\{X_t\}_{t\geq 0}$, taking its values from a finite set of integers, E. We call E the state space and denote its elements by $i, j, \ldots$. If for all integers $t \geq 0$ and all states $i, j, \ldots \in E$,

$$P(X_{t+1} = j | X_t = i, X_{t-1} = i_{t-1}, \ldots X_0 = i_0) = P(X_{t+1} = j | X_t = i) \tag{1}$$

then the stochastic process is called a Markov chain (for a general review, see, for example, *Bremaud* [1998]). The probabilistic dependence of Markov chains on the past is only through the previous state, and is expressed by the transition matrix $\mathbf{A} = \{a_{ij}\}_{i,j\in E}$, where

$$P(X_{t+1} = j | X_t = i) = a_{ij}. \tag{2}$$

At each discrete time step the Markov chain may therefore either remain in its present state, or transition to a new state, with probabilities defined by the elements of the transition matrix.

[12] Now consider a second process that generates a sequence of conditionally independent random variables, $\{O_t\}$, given the Markov chain, $\{X_t\}$, such that

$$P(O_{t+1} = y | X_{t+1} = j) = b_j(y), \quad j \in E, \quad y \in \Re. \tag{3}$$

[13] These two stochastic processes define a hidden Markov process (i.e., hidden Markov model). In this paper I use two interchangeable notations for these stochastic processes. When the temporal dependence of the processes is being emphasized, I use the notation introduced above (i.e., $\{X_t\}$, and $\{O_t\}$). When describing the model fitting process, for convenience I use vector notation (i.e., $\boldsymbol{X}$, and $\boldsymbol{O}$).

[14] The parameters of a hidden Markov model are defined by $\boldsymbol{\lambda} = [\boldsymbol{p}, \mathbf{A}, \boldsymbol{b}]$, where $\boldsymbol{p}$ is the initial probability distribution

$$p(i) = P(X_1 = i), \qquad i \in E, \tag{4}$$

$\mathbf{A}$ is the transition matrix of the Markov chain from (2), and $\boldsymbol{b}$ are the conditional probability density functions from (3), which can be either discrete or continuous. HMMs thus provide a means to model time series data that transition between states with distinct probability distributions.

2.2. State Space Probability Distributions for Hydrothermal Flow

[15] In many, if not most, applications, Gaussian densities are used for the conditional probability distributions, $\boldsymbol{b}$, in (3). Gaussian densities are mathematically convenient, but they may not be an appropriate choice for modeling hydrothermal flow records. Population distributions for hydrothermal flow records have not been widely studied nor reported, but recent work has shown that exit fluid temperature data from the active TAG hydrothermal mound are distinctly non-Gaussian [*Sohn*, 2007]. The TAG records exhibit skewed, long-tailed, and multipeaked histograms, with an overall correlation between the data mean and variance. These characteristics suggest that the data may be fit using mixtures of Gamma densities, which are flexible enough to model a wide range of population distributions, include an explicit correlation between mean and variance, and, like many flow records, have strictly positive values.

[16] Using Gamma densities for the conditional probability distributions of a hidden Markov model complicates numerical aspects of the model-fitting procedure, as we shall see below, but it provides a flexible class of signal models that may potentially be applied for a wide range of hydrothermal settings. If the conditional distribution of O_t given $X_t = j$ is Gamma(η_j, ν_j), we then have

$$b_j(y) = \frac{\eta_j^{\nu_j}}{\Gamma(\nu_j)} y^{\nu_j - 1} e^{-\eta_j y}, y \geq 0, j \in E, \tag{5}$$

where $\Gamma(\cdot)$ is the Gamma function. The Gamma pdf is defined by the so-called shape (ν_j) and scale (η_j) parameters. Varying ν changes the shape of the density, whereas varying η does not affect the shape but changes the values along the *x axis*, which is equivalent to changing the units of measurement (e.g., meters to kilometers). Note that the exponential density is a special case of the Gamma where $\nu = 1$, and the chi-square density with n degrees of freedom is also a special case of the Gamma where $\nu = n/2$ and $\eta = ½$.

2.3. Maximum Likelihood Model Fitting

[17] The Baum algorithm [e.g., *Baum and Petrie*, 1966], which is a special case of the expectation maximization (EM) algorithm of *Dempster et al.* [1977], is commonly used to fit a hidden Markov model to a sequence of observations. The method is guaranteed to converge to a local maximum in the log likelihood function if the logb_j are strictly concave over the parameter space. *Baum and Eagon* [1967] showed that the log-concavity condition holds for the Gamma density.

[18] To find the best fitting model $\boldsymbol{\lambda} = [\boldsymbol{p}, \mathbf{A}, \boldsymbol{b}]$ for an observation sequence $\{O_t\}$ of length T, we seek to maximize the likelihood function $\boldsymbol{\mathcal{L}}(\boldsymbol{O}|\boldsymbol{\lambda})$, which is done iteratively through forward and backward inductive computations in t. Let $\alpha_t(i) = \boldsymbol{\mathcal{L}}(O_1, O_2 \cdots, O_t, X_i|\lambda)$ and $\beta_t(i) = \boldsymbol{\mathcal{L}}(O_{t+1}, O_{t+2}, \cdots, O_T|X_i, \lambda)$ be defined as the forward, and backward, likelihoods, respectively. The forward likelihood is initialized as

$$\alpha_1(i) = p(i) b_i(O_1), \qquad 1 \leq i \leq n, \tag{6}$$

and induction leads to the recursive relationship,

$$\alpha_{t+1}(j) = \sum_{i=1}^{n} \alpha_t(i) a_{ij} b_j(O_{t+1}), \quad 1 \leq t \leq T-1; 1 \leq j \leq n. \tag{7}$$

Similarly, the backward likelihoods, after being arbitrarily initialized to one by convention (i.e., $\beta_T(i) = 1$, $1 \leq i \leq n$) are computed recursively from

$$\beta_t(i) = \sum_{j=1}^{n} \beta_{t+1}(j) a_{ij} b_j(O_{t+1}), \quad T-1 \geq t \geq 1; 1 \leq i \leq n. \tag{8}$$

The complete likelihood function can be expressed using the partial likelihoods above as

$$\boldsymbol{\mathcal{L}}(\mathbf{O}|\boldsymbol{\lambda}) = \sum_{i=1}^{n} \sum_{j=1}^{n} \alpha_t(i) a_{ij} b_j(O_{t+1}) \beta_{t+1}(j) \text{ for any } t \in [1, T-1]. \tag{9}$$

[19] The Baum algorithm can be implemented by taking the partial derivatives of the log likelihood function with respect to the model parameters $\boldsymbol{\lambda} = [\boldsymbol{p}, \mathbf{A}, \boldsymbol{b}]$, resulting in the so-called reestimation equations. The reestimation equations are used to iteratively update the model parameters until a stopping point is reached when the likelihood function converges to a maximum value. The reestimation equations for the initial distribution and transition probabilities are well known and do not depend on the state density functions except through the partial probabilities. The estimate for the initial distribution, $\bar{\boldsymbol{p}}$, is given by

$$\bar{p}(i) = \frac{\alpha_1(i)\beta_1(i)}{\sum_{i=1}^{n} \alpha_1(i)\beta_1(i)} = \frac{\alpha_T(i)}{\sum_{i=1}^{n} \alpha_T(i)}, \tag{10}$$

and the transition matrix, $\overline{\boldsymbol{A}}$, is given by

$$\bar{a}_{ij} = \frac{\sum_{t=1}^{T-1} \alpha_t(i) a_{ij} b_j(O_{t+1}) \beta_{t+1}(j)}{\sum_{t=1}^{T-1} \alpha_t(i)\beta_t(i)} = \frac{\sum_{t=1}^{T-1} \alpha_t(i) a_{ij} b_j(O_{t+1}) \beta_{t+1}(j)}{\sum_{t=1}^{T-1} \sum_{j=1}^{n} \alpha_t(i) a_{ij} b_j(O_{t+1}) \beta_{t+1}(j)}. \tag{11}$$

[20] The reestimation equations for the Gamma density parameters for each state are formed by taking partial derivatives and setting to zero, i.e.,

$$\frac{\partial \mathcal{L}(\boldsymbol{O}|\boldsymbol{\lambda})}{\partial \eta_j} = 0, \frac{\partial \mathcal{L}(\boldsymbol{O}|\boldsymbol{\lambda})}{\partial \nu_j} = 0.$$

For the scale parameter, η_j, we have

$$\frac{\partial \mathcal{L}}{\partial \eta_j} = \sum_{t=1}^{t-1} \sum_{i=1}^{n} \alpha_t(i) a_{ij} \left[\frac{\partial}{\partial \eta_j} b_j(O_{t+1}) \right] \beta_{t+1}(j), \tag{12}$$

where the term in brackets is evaluated using the result that

$$\left. \frac{\partial b_j}{\partial \eta_j} \right|_x = b_j(x) \left[\frac{\nu_j}{\eta_j} - x \right]. \tag{13}$$

Substituting and setting (12) to zero, we obtain

$$\sum_{t=1}^{T-1} \sum_{i=1}^{n} \alpha_t(i) a_{ij} b_j(O_{t+1}) \beta_{t+1}(j) \left(\frac{\nu_j}{\eta_j} \right) = \sum_{t=1}^{T-1} \sum_{i=1}^{n} \alpha_t(i) a_{ij} b_j(O_{t+1}) \beta_{t+1}(j) O_{t+1}, \tag{14}$$

which leads to

$$\bar{\eta}_j = \frac{\nu_j \sum_{t=1}^{T-1} \alpha_t(j) \beta_t(j)}{\sum_{t=1}^{T-1} O_{t+1} \sum_{i=1}^{n} \alpha_t(i) a_{ij} b_j(O_{t+1}) \beta_{t+1}(j)} = \frac{\nu_j \sum_{t=1}^{T-1} \sum_{i=1}^{n} \alpha_t(i) a_{ij} b_j(O_{t+1}) \beta_{t+1}(j)}{\sum_{t=1}^{T-1} O_{t+1} \sum_{i=1}^{n} \alpha_t(i) a_{ij} b_j(O_{t+1}) \beta_{t+1}(j)}. \tag{15}$$

[21] The procedure is somewhat more complicated for the shape parameter, ν_j, as taking the partial derivative necessarily involves differentiating the Gamma function in the denominator of the Gamma density. After taking $\frac{\partial \mathcal{L}}{\partial \nu_j}$ and setting to zero, we obtain

$$\psi(\bar{\nu}_j) = \frac{\sum_{t=1}^{T-1} \log\left(\eta_j O_{t+1}\right) \sum_{i=1}^{n} \alpha_t(i) a_{ij} b_j(O_{t+1}) \beta_{t+1}(j)}{\sum_{t=1}^{T-1} \sum_{i=1}^{n} \alpha_t(i) a_{ij} b_j(O_{t+1}) \beta_{t+1}(j)}, \tag{16}$$

where ψ is the digamma function [cf. *Levinson*, 1986]. Since $\psi(x)$ is strictly monotonic increasing and can be obtained by a power series for $x \in \Re^+$, (16) can be used to generate a reestimation equation for ν_j. Newton's method can be used to obtain

$$\nu_j^{k+1} = \nu_j^k - \frac{\psi\left(\nu_j^{(k)}\right) - \mathcal{C}}{\psi'\left(\nu_j^k\right)}, \tag{17}$$

where the superscripts are iteration number, the constant C is the right-hand side of (16), and $\psi'(\cdot)$ is the trigamma function. Power series can be used to obtain values for the digamma and trigamma functions [e.g., *Abromovitz and Stegun*, 1965].

2.4. Best Fitting State Sequence

[22] Another problem of interest is that of finding the best fitting state sequence for the Markov chain given an observation sequence and a model. The state sequence decodes the observations into a simpler set of integer variables drawn from the state space. Formally, we seek to maximize $\mathcal{L}(\boldsymbol{X}, \boldsymbol{O}|\boldsymbol{\lambda})$, which can be accomplished using the Viterbi algorithm [*Viterbi*, 1967]. To find the single best state sequence, $\boldsymbol{X}^* = \{X_1, X_2, \ldots, X_T\}$, we first define the quantity

$$\delta_t(i) = \max_{X_1, X_2 \ldots, X_{t-1}} \mathcal{L}(X_1, X_2, \cdots X_t = i, O_1, O_2, \cdots O_t|\lambda). \tag{18}$$

We interpret $\delta_t(i)$ as the highest probability along a single state sequence at time t, which accounts for the first t observations and ends in state X_i. By induction we have

$$\delta_{t+1}(j) = \left[\max_i \delta_t(i) a_{ij} \right] \cdot b_j(O_{t+1}). \tag{19}$$

To retrieve the state sequence, we need to keep track of the argument that maximized (19) for each t and j, which is done by introducing the array $\xi_t(j)$.

[23] Similar to the forward partial probability calculations (7)–(8), we initialize the recursive calculation with

$$\delta_t(i) = p(i) b_i(O_1), \quad 1 \le i \le n$$

$$\xi_1(i) = 0.$$

We then step forward through t using the recursive relationship

$$\delta_t(j) = \max_{1 \le i \le n} \left[\delta_{t-1}(i) a_{ij} \right] \cdot b_j(O_t), \quad 2 \le t \le T, 1 \le j \le n; \tag{20a}$$

$$\xi_t(j) = \arg \max_{1 \le i \le n} \left[\delta_{t-1}(i) a_{ij} \right], \quad 2 \le t \le T, 1 \le j \le n. \tag{20b}$$

The calculations terminate with

$$\mathcal{L}^* = \max_{1 \le i \le n} [\delta_T(i)] \tag{21a}$$

$$X_T^* = \arg \max_{1 \le i \le n} [\delta_T(i)]. \tag{21b}$$

To retrieve the optimum state sequence, we must then backtrack in t to find

$$X_t^* = \xi_{t+1}\left(X_{t+1}^*\right), \quad t = T-1, T-2, \cdots, 1. \tag{22}$$

[24] Both the Baum and Viterbi algorithms require scaling methods for successful implementation when there are more than a few observations. This results from the fact that the partial probabilities in the recursive equations (7)–(8) and (19)–(20) tend to zero exponentially fast in t, resulting

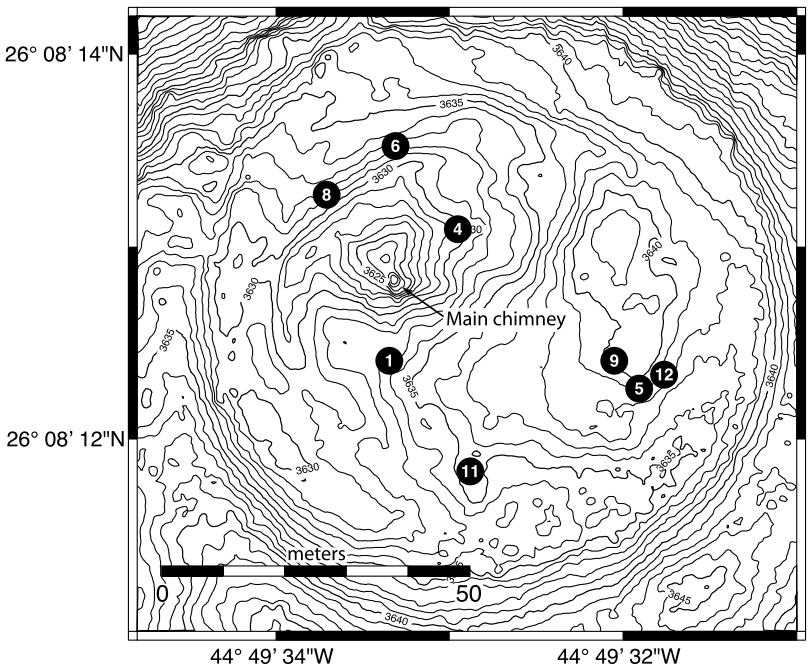

Figure 1. Bathymetry of the upper terrace of the TAG active hydrothermal mound and temperature probe positions. The main chimney and central black smoker complex are located slightly off center (to the northwest) on the ~100 m diameter upper terrace, shown here at the 1 m contour level from the gridded data of *Roman and Singh* [2007]. The time series temperature records modeled in this paper were acquired at the diffuse flow sites indicated by the numbered black circles.

in machine underflow errors in most real applications. An effective method for scaling the recursive equations to avoid underflow errors owing to *Levinson et al.* [1983] is described in Appendix B.

3. Application to Diffuse Flow Temperature Records From TAG

[25] I apply the maximum likelihood fitting method described above to fit HMMs to exit fluid temperature records acquired from the active TAG hydrothermal mound to demonstrate their utility as stochastic signal models for hydrothermal flow. The temperature records are described by *Sohn* [2007], but here I summarize the salient aspects of the data from the point of view of this research. Exit fluid temperature probes were deployed at 9 sites of high-temperature black smoker flow and 12 sites of low-temperature diffuse flow using DSRV *Alvin* in June 2003. The probes were recovered using ROV *Jason 2* in November 2004, and flow records were obtained for seven high-temperature and nine low-temperature sites (some probes were lost or destroyed during the deployment). All of the high-temperature and one of the low-temperature temperature records were clipped over significant time intervals, which limits their utility for stochastic analysis. For this analysis I selected diffuse flow records from the eight sites shown in Figure 1. The time series data, which are shown in Figure 2, sample temperature every 8 min over a period of 362 days from 27 June 2003 to 24 June 2004. Note that the first ~70 days of data for site 4 have been removed from the time series because of clipping issues.

3.1. Background Temperature Measurements

[26] The resolution of the VEMCO probes used to measure diffuse exit fluid temperatures at TAG was 0.2°C, which is roughly 4*x* the amplitude of background bottom water temperature variations of ~0.05°C measured with a SeaBird SBE 26 Deep-Sea Tide Gauge during the flow monitoring experiment [*Reves-Sohn et al.*, 2006]. This mismatch led to digitization issues during periods when the diffuse flow sites being monitored were not discharging hot water, and were thus measuring background temperature variations (see *Sohn* [2007] for details). As a result, all of the background temperature measurements at a given site fall into a single bin of the data logger (in a few cases background values alternate between two bins). Temperature measurements made during periods of background variability are thus underdiscretized, which, as I describe in section 3.3, is problematic for the model fitting procedure.

[27] To address this digitization issue, I first normalize the records to a background level of zero by subtracting the value of the data bin representing background temperature from each record, such that the records represent temperature anomaly above background (i.e., $dT \geq 0$). In cases where the background values are distributed between two bins, these data were combined into a single bin (with a value representing the arithmetic average of measurements from the two bins) before the background value was subtracted. I then use a point mass distribution, rather than a Gamma density, to model the background "no discharge" state. This is needed to prevent the model-fitting procedure from trying to converge on infinitely narrow and infinitely tall "delta functions" centered on individual data bins for records with large fractions of data at background temper-

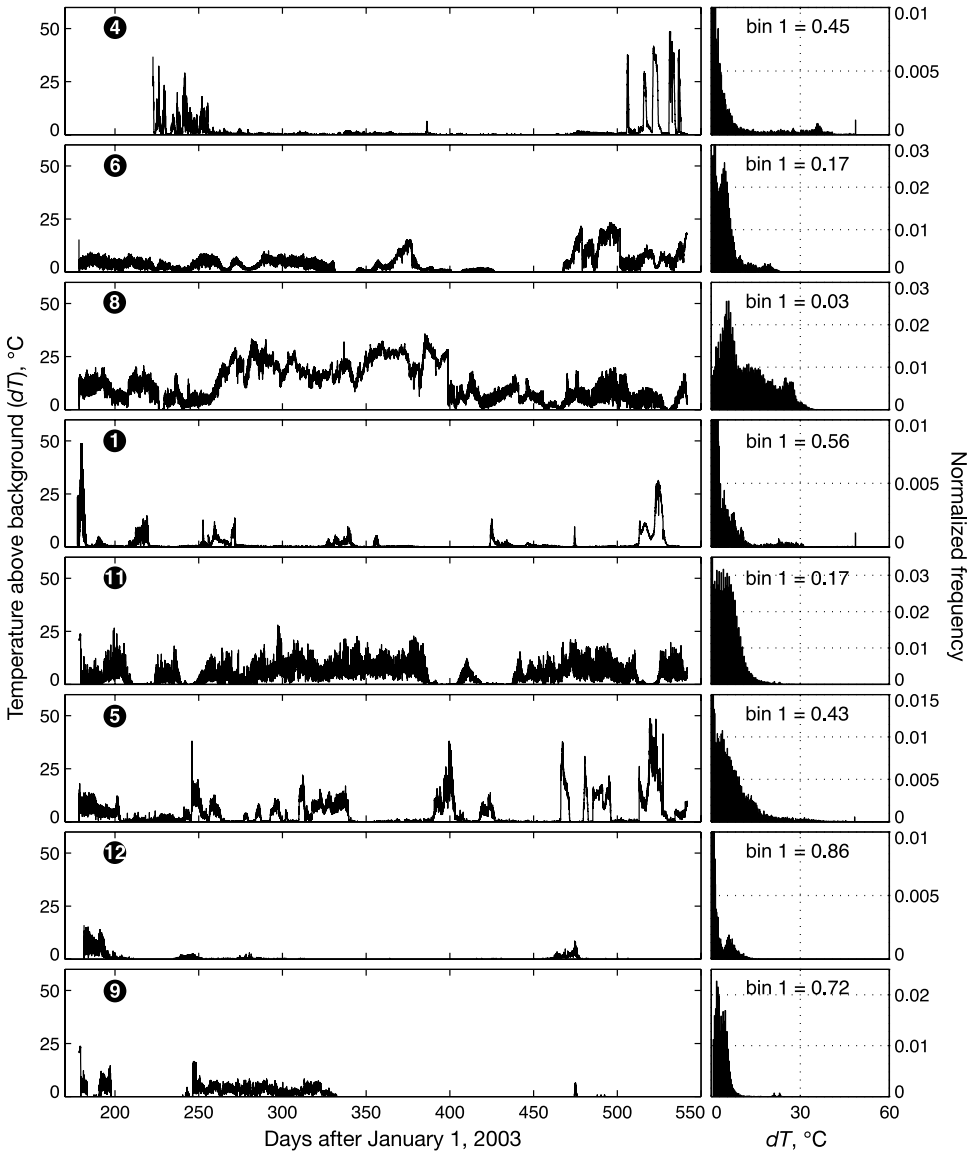

Figure 2. Exit fluid temperature time series data and histograms. (left) Time series records for each diffuse flow site and (right) the corresponding data histograms. The probe numbers correspond to the positions from Figure 1, and the vertical alignment from top to bottom represents a counterclockwise progression around the mound. The time series data are plotted on a common scale, but the y axes of the histograms are scaled differently for each record. The histogram bins correspond directly to the data logger bins, and the y axis counts are normalized to 1, such that the fraction of total observations in each bin is plotted. The fraction of observations in the first data bin, which is off scale for all of the records except for 8, is listed on each histogram.

ature levels (see section 3.3). The complete set of density functions are thus

$$\begin{aligned} b_1(y) &= 0, & y &\neq 0, \\ b_1(y) &= 1, & y &= 0, \\ b_j(y) &= 0, & y &= 0, 2 \leq j \leq n, \\ b_j(y) &= \frac{\eta_j^{\nu_j}}{\Gamma(\nu_j)} y^{\nu_j - 1} e^{-\eta_j y}, & y &\neq 0, 2 \leq j \leq n, \end{aligned} \tag{23}$$

where n is the number of states in the space E.

3.2. Initial Values

[28] To use the reestimation equations (10)–(11) and (15)–(17) to fit hidden Markov models to the exit fluid temperature time series data, we must first select a starting model, $\boldsymbol{\lambda}^0 = [\boldsymbol{p}^0, \mathbf{A}^0, \boldsymbol{b}]$. Initial values for the shape and scale parameters of the state densities, $\boldsymbol{b}^0$, can be estimated from the data histograms (Figure 2) utilizing the fact that the mean, or expected, value of the Gamma density is given by the ratio of the shape and scale parameters, $E(b_j) = \nu_j/\eta_j$. Individual peaks in the data histograms can thus be matched to starting values for Gamma density parameters based on their approximate mean value.

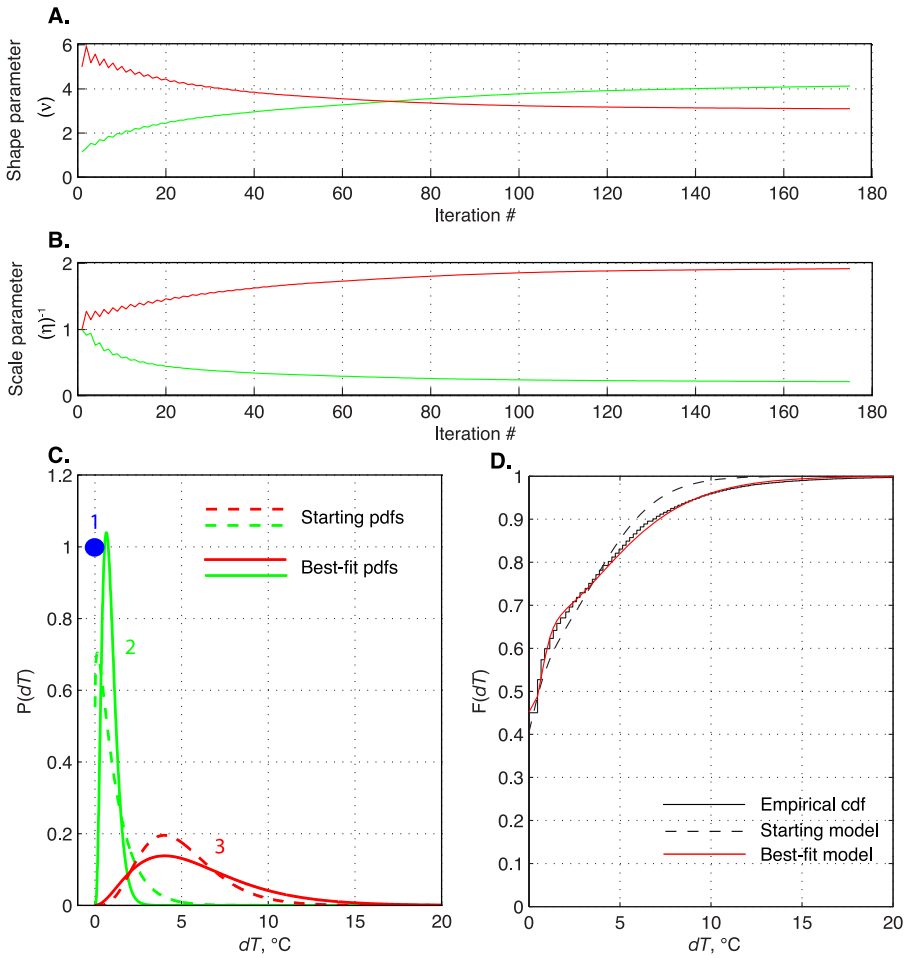

Figure 3. An example of the iterative model-fitting process. A three-state HMM is fit to the data from probe 5. (a) Shape and (b) scale parameters for the gamma state densities, converging to a final solution in 175 iterations. (c) Probability and (d) cumulative density functions of the starting and final model for comparison. Note the close match between the long-run behavior predicted by the cumulative density function (cdf) of the final model and the empirical cumulative density function of the data in Figure 3d. Note that the density function for state 1 is fixed as a point mass at zero.

[29] Initial values for the transition matrix, $\mathbf{A}^0$, can be generated by approximating the stationary distribution, $\boldsymbol{\pi}$, from the empirical cumulative distribution of the observation sequence, and then using stochastic constraints and the global balance equations to constrain the matrix elements. The stationary distribution characterizes the long-run statistics of the HMM. The probability model in (4) specifies that the first element of the stationary distribution, $\pi(1)$, is equal to the fraction of total observations in the first data bin, which is readily calculated. Estimates for the remaining elements of the stationary distribution can be approximated from the histograms. The stochastic constraints are

$$a_{ij} \geq 0, \sum_{1 \leq k \leq n} a_{ik} = 1. \tag{24}$$

We do not set any elements to exactly zero as it would a priori rule out the possibility of a transition between the corresponding state pair. The global balance equations are

$$\pi(i) = \sum_{1 \leq j \leq n} \pi(j) a_{ji}, \tag{25}$$

and (24) and (25) combine to produce an underdetermined set of linear equations for the transition matrix elements, reflecting the one-to-many relationship between stationary distributions and transition matrices. Any choice of transition matrix elements within the solution space of the linear equations suffices for the purpose of choosing initial values, provided none of the elements are initially set to zero.

[30] Selection of initial values for the initial distribution, $\boldsymbol{p}$, can be accomplished by guessing the value of the state variable corresponding to the first data point, $\hat{X}_1$, and setting $p\,(\hat{X}_1)=1$. $p(\neq\hat{X}_1)=0$. In practice, the fitting method is relatively insensitive to the initial values. The reestimation equations converge to the same best fitting model for a wide range of starting models, and in most cases the penalty for choosing a "bad" starting model is slow convergence. An example of the iterative fitting procedure and model convergence is shown in Figure 3.

3.3. Model Order and Selection

[31] The model order (i.e., number of states in the Markov process) is not known a priori, and we must

Table 1. Model-Fitting Statistics

Site	Probe	Statistic[a]	Minimum Value	Number of States in HMM[b]					
				2	3	4	5	6	7
9	1	BIC		-3.9×10^4	-3.2×10^4	-2.9×10^4	-2.6×10^4	x	x
		K-S	(5.7)	7.9	10.7	8.0	6.3	x	x
		C-vM	(5.3)	12.1	23.8	7.3	6.7	x	x
	2	BIC		-4.2×10^4	-3.6×10^4	-3.2v10^4	x	x	x
		K-S	(5.7)	7.6	11.1	9.0	x	x	x
		C-vM	(5.6)	10.1	25.3	8.5	x	x	x
12	1	BIC		-2.7×10^4	-1.7×10^4	-1.4×10^4	-1.2×10^4	x	x
		K-S	(10.5)	30.3	11.3	12.3	12.1	x	x
		C-vM	(10.1)	233.0	18.0	12.4	13.2	x	x
	2	BIC		-2.4×10^4	-1.7×10^4	-1.3×10^4	x	x	x
		K-S	(11.4)	13.9	12.8	14.0	x	x	x
		C-vM	(12.2)	56.7	23.4	15.5	x	x	x
5	1	BIC		-1.0×10^5	-7.7×10^4	-6.6×10^4	-5.9×10^4	-5.5×10^4	x
		K-S	(13.2)	19.7	15.2	15.6	15.9	16.1	x
		C-vM	(11.2)	62.1	23.2	19.9	14.8	13.8	x
	2	BIC		-1.2×10^5	-9.9×10^4	-8.5×10^4	-7.5×10^4	-6.9×10^4	-6.4×10^4
		K-S	(10.1)	13.6	11.3	11.8	11.9	12.3	12.3
		C-vM	(4.3)	20.6	23.9	19.0	10.2	7.9	5.8
11	1	BIC		-1.5×10^5	-1.3×10^5	-1.2×10^5	-1.1×10^5	-1.1×10^5	x
		K-S	(5.5)	19.1	9.8	8.4	7.0	7.1	x
		C-vM	(4.3)	71.3	15.2	12.3	7.8	5.1	x
	2	BIC		-1.5×10^5	-1.3×10^5	-1.2×10^5	-1.1×10^5	-1.1×10^5	x
		K-S	(5.5)	18.7	9.7	8.4	7.0	7.1	x
		C-vM	(4.3)	67.5	14.8	12.3	7.8	5.1	x
1	1	BIC		-6.3×10^4	-4.0×10^4	-3.2×10^4	-2.2×10^4	x	x
		K-S	(26.2)	33.3	26.4	31.6	26.4	x	x
		C-vM	(86.6)	344.9	133.0	102.8	88.9	x	x
	2	BIC		-7.7×10^4	-5.2×10^4	-4.0×10^4	-3.5×10^4	-3.1×10^4	x
		K-S	(22.4)	30.1	23.0	27.3	27.5	27.8	x
		C-vM	(51.4)	278.5	102.1	68.7	64.6	64.0	x
8	1	BIC		-2.2×10^5	-1.8×10^5	-1.6×10^5	-1.5×10^5	-1.4×10^5	x
		K-S	(3.3)	14.6	12.0	13.4	5.7	5.5	x
		C-vM	(1.0)	64.5	25.7	21.0	4.2	3.3	x
	2	BIC		-2.0×10^5	-1.6×10^5	-1.5×10^5	-1.3×10^5	x	x
		K-S	(4.2)	9.6	15.1	14.6	10.1	x	x
		C-vM	(2.2)	19.7	38.8	29.8	8.9	x	x
6	1	BIC		-1.3×10^5	-1.0×10^5	-8.6×10^4	x	x	x
		K-S	(9.1)	15.9	18.6	12.1	x	x	x
		C-vM	(6.6)	46.3	78.0	13.0	x	x	x
	2	BIC		-1.4×10^5	-1.2×10^5	-9.5×10^4	-8.5×10^4	x	x
		K-S	(5.6)	14.1	21.7	6.9	8.6	x	x
		C-vM	(3.1)	40.4	98.7	5.5	6.3	x	x
4	1	BIC		-6.1×10^4	-3.9×10^4	-2.7×10^5	-2.1×10^4	-1.6×10^4	x
		K-S	(12.1)	38.1	17.0	15.1	15.6	15.9	x
		C-vM	(19.9)	495.8	51.5	29.2	26.8	25.8	x
	2	BIC		-7.1×10^4	-4.4×10^4	-3.5×10^4	-2.9×10^4	-2.5×10^4	x
		K-S	(19.4)	39.6	20.2	22.8	24.2	22.0	x
		C-vM	(45.6)	478.8	69.2	69.1	58.1	49.4	x

[a]BIC, Bayesian information criterion; K-S, Kolmogorov-Smirnov test statistic $\sqrt{T}D_T$; C-vM, Cramer-von Mises test statistic $T\omega_T^2$.
[b]For number of states the x indicates unstable solution.

therefore consider the issue of model selection. Estimating the order of an HMM is a difficult problem. Bootstrap [e.g., *Ryden et al.*, 1998] methods sidestep the considerable complexities of the analytical problem, but for large data sets, such as the TAG temperature records, they are prohibitively expensive from a computational point of view. Bayesian approaches based on the likelihood are natural choices for the present application given that maximum likelihood methods were used for model fitting. We select the model with the highest value of an objective function that penalizes the likelihood by a factor related to the model dimension. The Akaike information criterion [*Akaike*, 1974] and Bayesian information criterion (BIC) [*Schwarz*, 1978] are two commonly used objective functions, and of these we prefer the latter given its suitability for large samples.

[32] I fit HMMs to each of the diffuse flow observation sequences using a range of model sizes, and BIC values for each best fit model are tabulated in Table 1 and plotted in Figure 4. In all cases BIC monotonically increases with the number of states until the solution becomes unstable. The instability results from the collapse of a Gamma pdf onto a single data bin, at which point the solver asymptotically moves toward an infinitely thin and tall ''delta function'' centered on the value of the data bin. This is the same digitization problem described for background temperature measurements described in section 3.1, and results from the use of continuous density functions to model underdiscre-

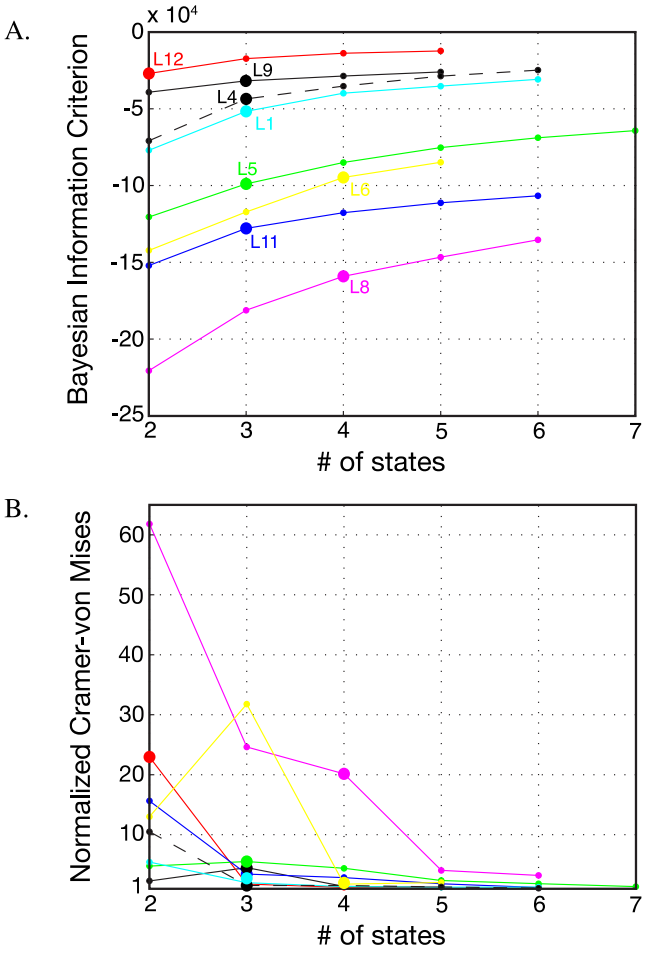

Figure 4. Model selection statistics.(a) Bayesian information criterion and (b) Cramer-von Mises statistics for each data record for best fit models employing between two and seven states.

tized data. The number of states for which numerical solution becomes unstable depends on the distribution of data values within the discrete data bins. Time series with large numbers of observations in a few data bins (i.e., flow mostly "off" sequences) are most susceptible to this problem, and in these cases the solution is unstable for $n \geq 5$. For all of the diffuse flow records from TAG the solution is unstable for $n \geq 8$.

[33] Given these digitization and numerical issues we cannot formally use BIC for model selection in this particular case. As an alternative we may consider comparing the empirical distribution of the data, $\hat{F}$, to the target distribution of the model, F_0. The long-run distribution of a hidden Markov model can be estimated as a mixture of the component pdfs using the stationary distribution, $\boldsymbol{\pi}$, of the transition matrix, $\mathbf{A}$, which allows the use of a distribution-free test, such as the Kolmogorov-Smirnov (K-S), or Cramer-von Mises (C-vM) statistics, to test $H{:}F = F_0$ against the null $H_0{:}F \neq F_0$.

[34] K-S and C-vM test statistics (equations provided in Appendix A) for each of the best fit models are tabulated in Table 1, and the C-vM statistics are plotted in Figure 4. Both statistics treat the data as an aggregate mixture of the state pdfs and thus, unlike BIC, do not consider serial correlations in the data. These statistics do, however, converge to asymptotic values faster than BIC as the number of states is increased. Unfortunately, critical values established for testing H against H_0 using the K-S and C-vM statistics cannot be used for these data because the asymptotic minimum values are limited by the multiple number of observations in each of the data bins (see Appendix A for governing equations).

[35] The theoretical and numerical difficulties described above preclude formal estimates of model order in this paper, but we can nevertheless see that models with between three and five states provide good fits for the diffuse flow time series data (Figures 4 and 5). The best fit models shown in Figure 5 were selected based on consideration of the BIC, K-S, and C-vM statistics, and it is clear that the number of states required to fit the data depends on the vigor of venting. Observation sequences with lots of background temperature values require fewer states than records with persistent exit fluid temperature anomalies. We also find that the expected temperature value for each state is similar for all sites across the mound and that the expected values increase roughly exponentially with increasing state number (Figure 6). This may prove to be a useful result for synoptic flow modeling using Markov processes and may also provide insight toward interpretation of state sequences, as I discuss in section 4. More sophisticated analyses, such as perhaps the reversible jump method [*Robert et al.*, 2000] or the penalized minimum distance method [*MacKay*, 2002], will be required to formally address the model selection issue in the future.

3.4. State Sequences for the Diffuse Flow Records

[36] I apply the Viterbi algorithm to the diffuse flow records using the best fitting models shown in Figure 5 to illustrate the process of state sequence estimation. The results are shown in Figure 7, where the time series data for each probe are color-coded by the best fitting state sequence, with the best fitting state sequence, itself, plotted underneath each temperature record. To first order, the state sequences provide a good indication of discharge patterns across the TAG mound, and the systematic relationship between expected values for the conditional density functions allows us to make general associations between discharge patterns and the state space, E. For example, for the three-state HMMs we can associate the state 1 with periods of no discharge, state 2 with periods of weak discharge, and state 3 with periods of vigorous (shimmering) discharge. This provides a convenient way to classify and model flow that could, in principle, be extended all the way up to black smoker discharge temperatures.

[37] Although Viterbi decoding provides a method for classifying the temperature observations into discrete discharge episodes, some problems with the state sequence estimates are apparent. Upon inspection we can see that there are time periods during which the state sequence alternates between two states even though the discharge temperature does not vary episodically. For example, there is a flow episode at site 11 between days 225 to 240, but the best fitting state sequence alternates between states 2 and 3, and even includes a brief excursion to state 1 (Figure 8). These kinds of "false" transitions in the state sequence are

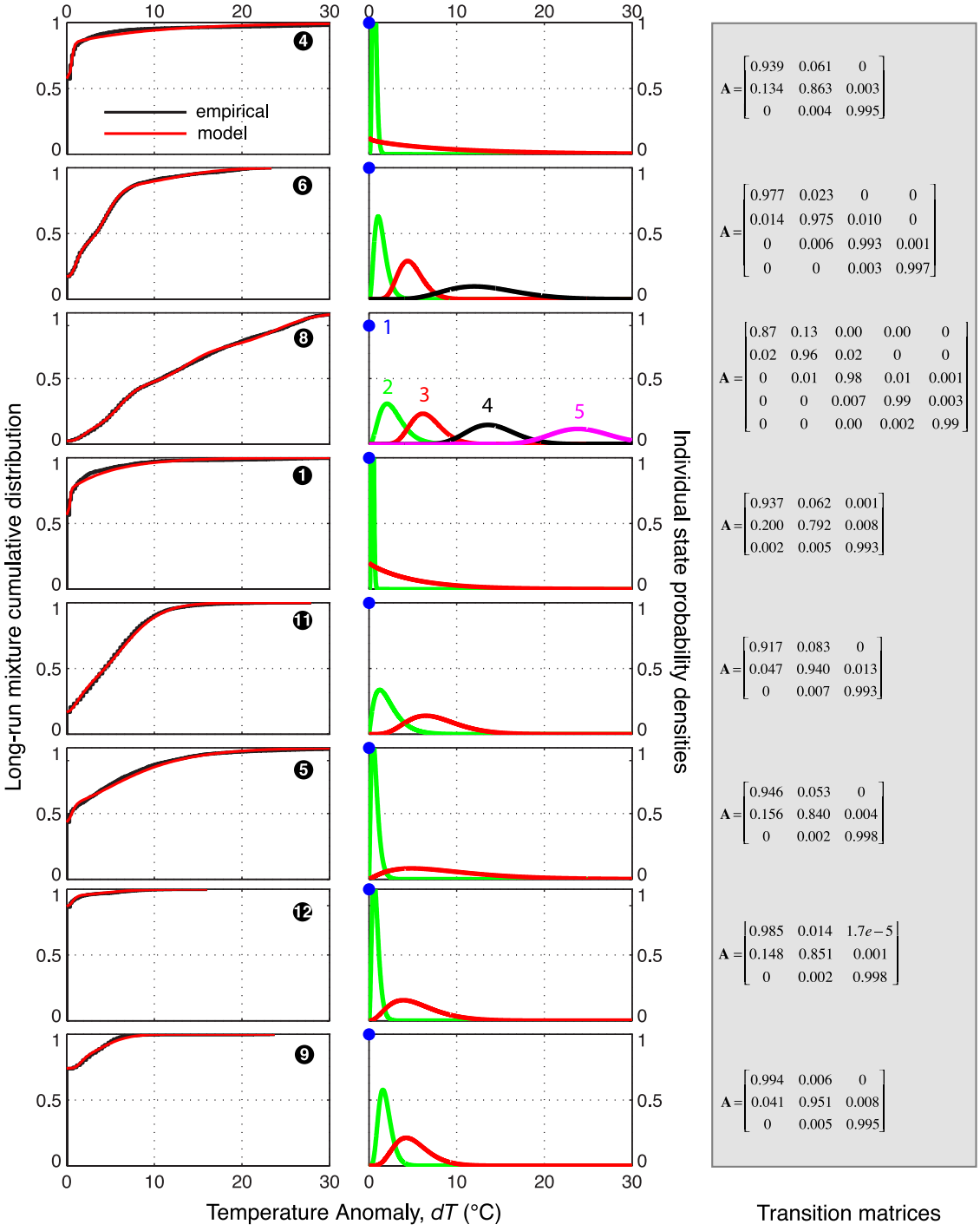

Figure 5. Best fit HMM for each temperature record (vertical alignment same as for Figure 2). (left) Comparison between the empirical cumulative distribution function and the long-run cumulative distributions for each record. (middle) Density functions for the final, color coded by state number (state 1 blue, state 2 green, state 3 red, state 4 black, state 5 magenta). (right) Transition matrices for the best fit models.

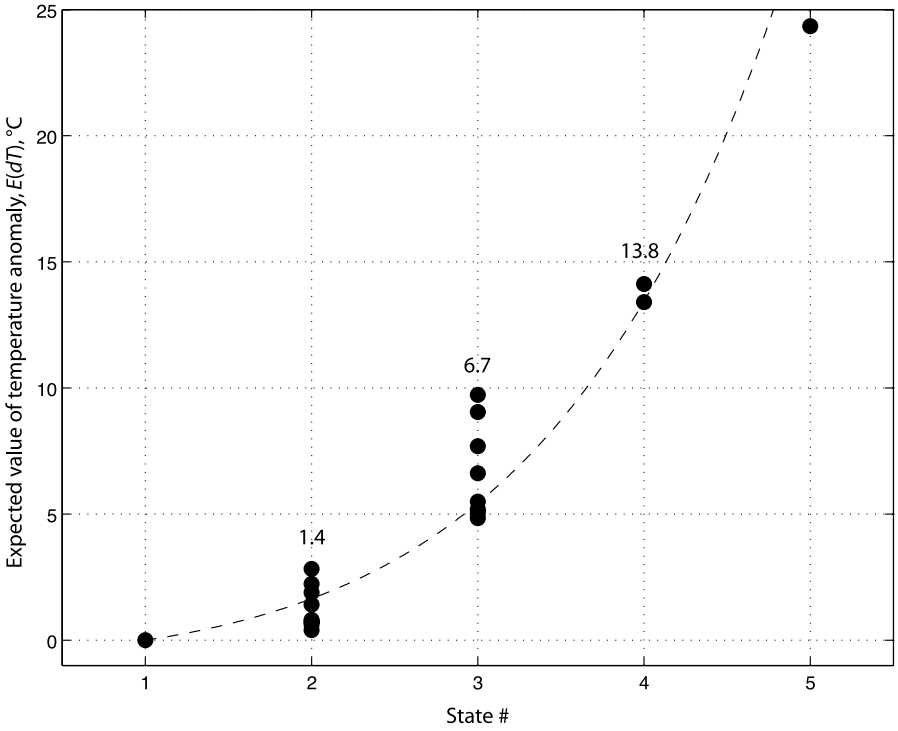

Figure 6. Expected values of the best fit model states. The average expected value for each state is listed above the data points. The roughly exponential increase in expected value with state number is shown by comparison with the dashed line plotting the function $E(b_j) = (j-1)\, e^{((j-1)/2)}$, where b_j is the density function for state j.

evident in all the records, and result from temperature variations that just exceed the nominal range of a given density function for a brief time, rather than a flow perturbation. I discuss some potential solutions to this problem, in section 4.

4. Summary and Discussion

[38] I have used hidden Markov models to develop a stochastic signal model for episodic modes of variability in hydrothermal flow records. The signal model is completely general and can thus be fit to any type of observation sequence (e.g., salinity, temperature) provided a suitable set of density functions can be identified. Reestimation equations for HMMs employing Gaussian density functions are widely available in the literature [e.g., *Ephraim*, 2002, and references therein], but here I have used Gamma densities because of their flexibility for modeling skewed, or exponential-type, flow records. HMMs employing Gamma state densities may be flexible enough to model a wide class of signals for strictly positive time series observations.

[39] I successfully applied HMMs to model diffuse flow exit fluid temperature time series data from the active TAG hydrothermal mound. The reestimation equations converged to a final model within a few hundred iterations unless the initial guesses were wildly in error. I modeled most (6 of 8) of the records using three-state HMMs, and used four- or five-state HMMs for sites of more vigorous and/or continuous discharge. These HMMs have between 10 and 28 total degrees of freedom (the relationship between number of states and model size is given in Appendix A), demonstrating that HMMs provide a compact and numerically efficient means to model the complex, episodic behavior observed in the temperature records from TAG. I was not able to obtain a formal statistical estimate of model order (i.e., number of states) for the temperature records using methods based on the likelihood, and this is an important topic for future research. Alternative methods will need to be explored [e.g., *MacKay*, 2002; *Robert et al.*, 2000; *Ryden et al.*, 1998].

[40] I experienced problems using continuous density functions to model the underdiscretized exit fluid temperature records from TAG. When a sufficiently large fraction of digital observations fall within a single data bin the maximum likelihood method will attempt to fit a "delta function" to the numerical value of the bin, and the solution becomes unstable. For the diffuse flow temperature records from TAG, large fractions (up to 86%) of the 65,408 time series measurements in each record can fall within a single data bin corresponding to the back groundwater column temperature value of $\sim$2.7°C, such that it was more appropriate to use a point mass, rather than Gamma, density to model this "background" flow state. I normalized the records to a background level of zero (by subtracting the value of the background bin from all the observations), and then used a point mass (at zero) density function for state 1 (equation (23)), which stabilized the numerical method over the solution space of interest (low-order models). These kinds of numerical issues should not be a problem for adequately digitized flow records. The data loggers in the VEMCO probes [*Fornari et al.*, 1994] used to monitor diffuse flow at TAG had only 128 data bits covering the

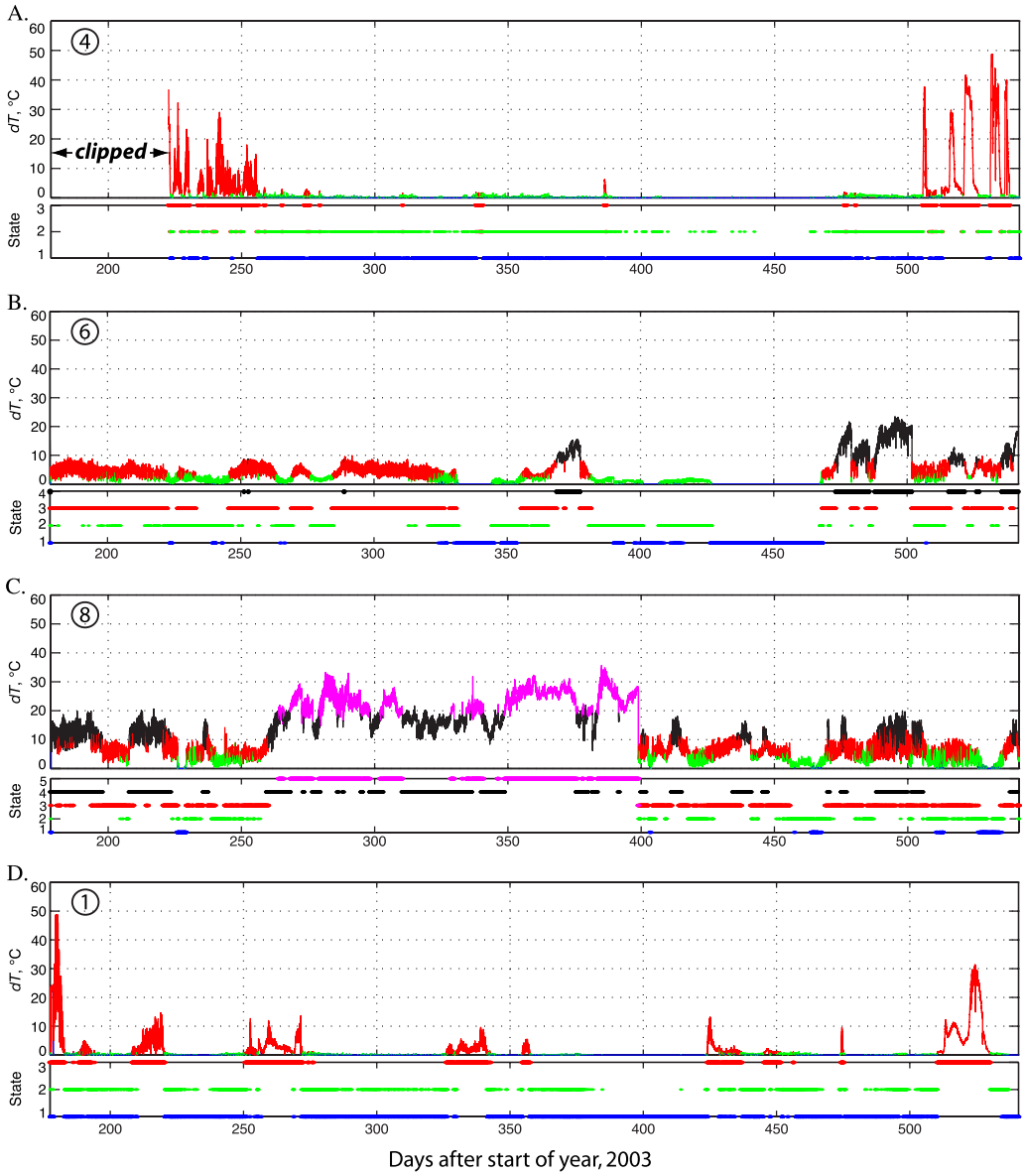

Figure 7. Application of the Viterbi algorithm to each temperature record using the best fit models from Figure 5. The time series data for each record are color coded by the best fitting state sequence estimate using the same color scheme as Figure 5 (i.e., state 1 blue, state 2 green, state 3 red, state 4 black, state 5 magenta). The best fitting state sequence, itself, is plotted underneath the time series data. A short segment of the time series from probe 11 (Figure 7e) is shown in Figure 8.

temperature range from 0 to 60°C (resolution of 0.2°C),which was insufficient for resolving the temperature variations at the diffuse flow sites.

[41] I used the Viterbi algorithm to estimate the best fitting state sequence for each of the diffuse flow exit fluid temperature records. The state sequence does not have a formal physical interpretation, but we may nevertheless make general associations between the state space and the vigor of discharge owing to the first-order correlation between expected values for the state densities (Figure 6). State 1 is hard-wired to represent a "no discharge" flow state, which could represent either no-flow or flow recharge conditions [*Sohn*, 2007]. State 2, with an expected value of 1–2°C, represents a "weak discharge" flow state. State 3, with an expected value of 5–10°C, represents a more vigorous state of diffuse discharge, and so on. The roughly exponential increase in the expected temperature value with model state implies that it may be possible to extend the models to high-temperature (e.g., black smoker) venting using models with eight to nine flow states. This result has implications for synoptic flow models, as described below, but the suitability of HMMs as signal models for black smoker flow records remains to be determined.

[42] The state sequence may potentially be used to identify flow events based on the timing of state transitions. Transition times are a point process that could be correlated with events in a geological record, such as a seismicity catalogue, and thereby provide an objective means to identify event pairs for perturbation response analysis. Inspection of the state sequences in Figure 7, however,

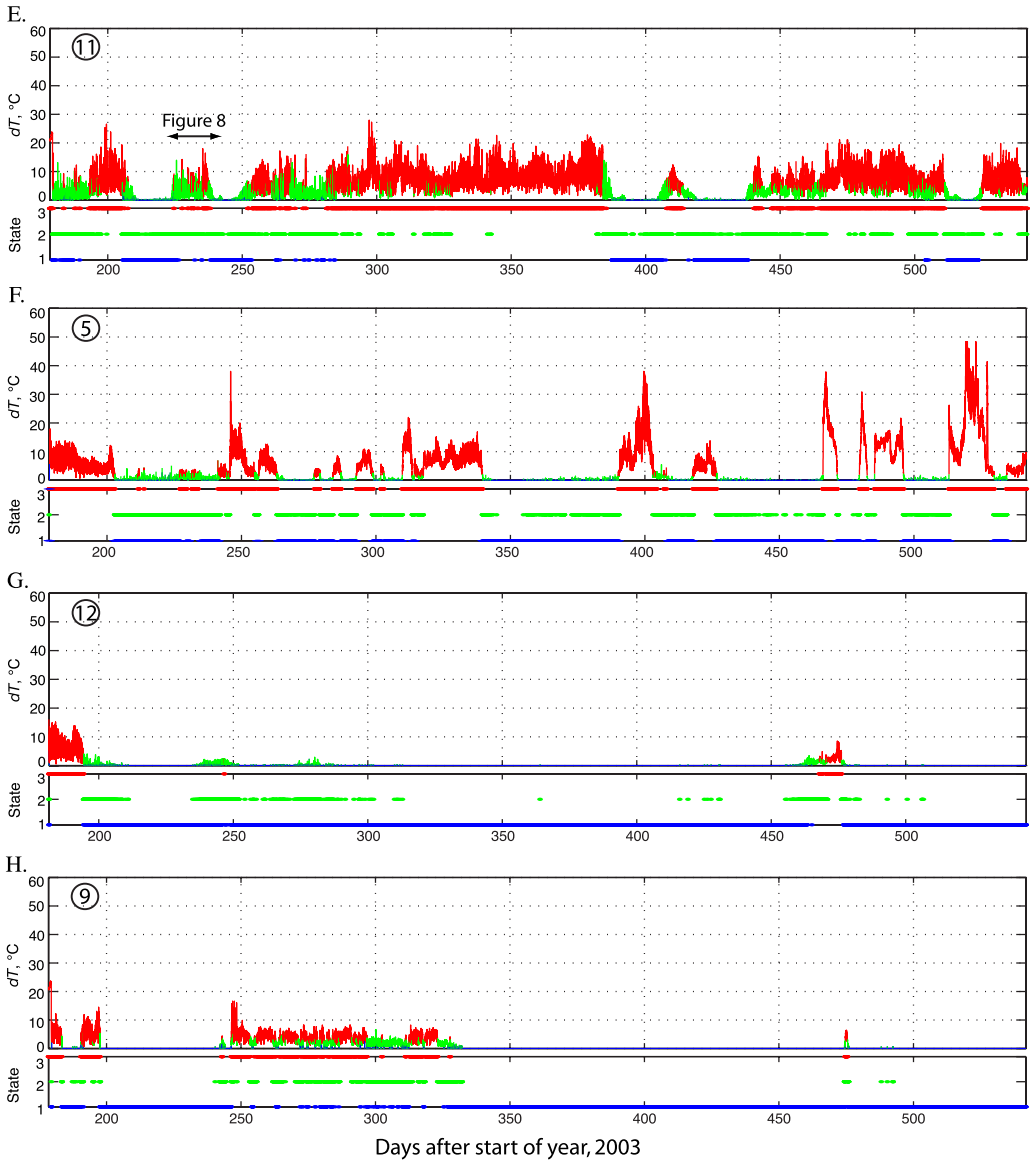

Figure 7. (continued)

demonstrates that additional research will be required before this kind of analysis is possible. In many cases the best fitting state sequence for diffuse flow temperature records at TAG transitions back and forth between two flow states during times when the presence of episodic variations is unclear. An example of this situation is shown in Figure 8. This behavior is partly attributable to the fact that not all variations in the temperature records are episodic. For example, tidal forces generate harmonic variations in the time series data that are not incorporated into the HMM signal model. The tidal pulsing phenomenon described by *Sohn* [2007] is observed for the first ~3 days of the record shown in Figure 8, and this generates periodic transitions between states 1 and 2 for several days. These transitions are not associated with episodic perturbations from geological processes, but instead result from tidal forcing which generates transitions between periods of flow discharge and recharge at a site of low net fluid flux [e.g., *Crone and Wilcock*, 2005].

[43] Ultimately we may hope to incorporate harmonic modes of variability into a stochastic flow model, but there are several ways to stabilize the state sequence estimates without taking this step. Perhaps the simplest solution is to filter out harmonic variability from the observation sequence or the best fitting state sequence. This approach may work well if the passband of harmonic variability is either at the low end of the frequency spectrum or very narrow, but filtering can affect the apparent timing and amplitude of impulse or step-like flow events, and therefore must be applied carefully. A more difficult, but possibly more appealing, alternative would be to use continuously variable duration hidden Markov models (CVDHMMs) as a signal model [e.g., *Levinson*, 1986]. In a traditional HMM, the probability of duration of a state decreases exponentially with time. The probability of remaining in state j, for duration, D, (discrete time steps), $\boldsymbol{Pr}\,[D|j]$ is proportional to a_{jj}^{t-1}. This exponential distribution may not be appropriate for hydrothermal flow records, particularly if the sample

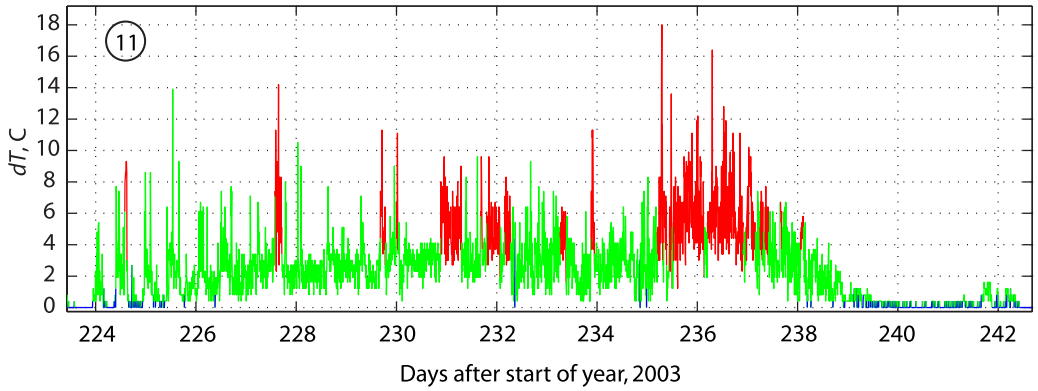

Figure 8. Blowup of days 224–242 from probe 11 (see Figure 7e) illustrating classification problems for the state sequence estimate. The time series is color coded by state sequence as for Figure 7. The flow episode is seen to initiate with semidiurnal oscillations that clip low at the back groundwater column temperature (i.e., dT = 0) for the first 1.5 days (this is the "chugging" behavior described by *Sohn* [2007]. The state sequence estimate jumps back and forth between states 1 and 2 during this time period. Later on, during the flow episode, the state sequence estimate alternates between states 2 and 3 during temperature variations that are not necessarily indicative of episodic perturbations. These kinds of "nonepisodic" state transitions can present issues for interpretation of the state sequence.

interval is much smaller than the duration of flow episodes, as is the case for the diffuse flow data from TAG. CVDHMMs address this issue by using a separate set of density functions to model state duration, which can stabilize the state sequence during long flow episodes under an appropriate parameterization, thereby providing a means to avoid "false transitions" in the state sequence.

[44] I have applied HMMs to flow records from individual sites, but an important step will be to incorporate the time-space correlation between simultaneously acquired records into a synoptic stochastic flow model. Most of the commonly used methods for quantifying spatial correlation in subaerial hydrologic systems (e.g., semivariograms) are not appropriate for a signal model based on Markov processes, which is not stationary in the traditional sense. Alternate techniques, such as perhaps Markov Random Fields, will be required to model the space-time variability of a Markovian signal. However, if this important step can be taken, then we can use the resulting stochastic models to estimate the statistical moments of important subsurface flow parameters, such as velocity, permeability, and pressure [*Rubin*, 2003], and thereby constrain subsurface flow patterns without having to model all of the complex interactions between the physical and chemical processes that govern hydrothermal flow. This kind of stochastic modeling has not yet been attempted for deep-sea hydrothermal systems, but the signal model developed in this work may represent an important step toward this objective.

Appendix A: Model Selection Statistics

[45] The Bayesian information criterion [*Schwarz*, 1978] is given by

$$BIC = \log \mathcal{L}_n - \frac{1}{2} k_n \log T, \tag{A1}$$

where $\mathcal{L}_n$ is the likelihood function of the best fitting model with n states, T is the number of data points, and k_n is the model dimension. The dimension of an n state HMM for a two-parameter density family is $k_n = (n-1)n + 2n$ [*Ryden*, 1995], which must be modified to $k_n = (n-1)\,n + 2\,(n-1)$ to account for the point mass distribution of state one.

[46] The Kolmogorov-Smirnov statistic is given by

$$D_T = \max_{i=1,\ldots,T} \max\left\{ \frac{i}{T} - F_0\left(O_{(i)}\right) F_0\left(O_{(i)}\right) - \frac{(i-1)}{T} \right\}, \tag{A2}$$

where the $O_{(i)}$ are the order statistics $O_{(1)} < O_{(2)} < \ldots < O_{(T)}$, and F_0 is the cumulative density function of the best fit model. Similarly, the Cramer-von Mises statistic is computed as

$$\omega_T^2 = \frac{1}{12T^2} + \frac{1}{T} \sum_{i=1}^{T} \left\{ F_0\left(O_{(i)}\right) - \frac{(2i-1)}{2T} \right\}^2. \tag{A3}$$

Critical values established for the Kolmogorov-Smirnov and Cramer-von Mises statistics strictly require $O_{(1)} < O_{(2)} < \ldots < O_{(T)}$. When individual data bins contain multiple observations (i.e., $O_{(1)} \leq O_{(2)} \leq \ldots \leq O_{(T)}$) the asymptotic minimum values of the test statistics are given by

$$D_T^{\min} = \frac{\left(\max n_{b(i)}\right)}{2T} \tag{A4}$$

and

$$\omega_T^{2,\min} = \frac{1}{12T^2} + \frac{1}{T} \sum_{i=1}^{b_N} \left\{ \omega_i^2 \right\}^2, \tag{A5}$$

where

$$\omega_i^2 = \sum_{j=1}^{n_{b(i)}} \left\{ \frac{\left(2j - n_{b(i)} - 1\right)}{2T} \right\}^2, \tag{A6}$$

b_N is the number of data bins, and $n_{b(i)}$ is the number of observations in bin (i). These minimum values for each observation sequence are listed in Table 1.

Appendix B: Scaling

[47] The recursive equations (equations (7)–(8) and (19)–(20)) tend to zero exponentially fast in t when there are more than a few observations, resulting in machine underflow errors in most real applications (there are 65480 observations in each low-temperature time series). *Levinson et al.* [1983] described effective scaling methods for both the Baum and Viterbi algorithms. For the Baum algorithm we define a set of scaling coefficients

$$c_t = \frac{1}{\sum_{i=1}^{n} \alpha_t(i)}. \tag{B1}$$

The partial likelihoods of equations (7)–(8) are then written as

$$\alpha_{t+1}(j) = \sum_{i=1}^{n} \hat{\alpha}_t(i) a_{ij} b_j(O_{t+1}) \tag{B2}$$

and

$$\beta_t(i) = \sum_{j=1}^{n} \hat{\beta}_{t+1}(j) a_{ij} b_j(O_{t+1}) \tag{B3}$$

where

$$\hat{\alpha}_t(i) = c_t \alpha_t(i) \tag{B4}$$

$$\hat{\beta}_t(j) = c_t \beta_t(j). \tag{B5}$$

The reestimation equations can then be written in terms of the scaled partial likelihoods. The scaled reestimation equations yield the correct values because the products of scale factors used to avoid underflow cancel each other out exactly in the numerator and denominator.

[48] For the Viterbi algorithm we use logarithms to scale the recursive calculations. As an alternative to equation (20), we define

$$\phi_t(i) = \max_{X_1, X_2, \ldots, X_{t-1}} \{\log \boldsymbol{\mathcal{L}}(X_1 X_2 \ldots X_t = i, O_1 O_2 \ldots O_t | \lambda)\}. \tag{B6}$$

We then initialize the recursion with

$$\phi_t(i) = \log(\pi_i) + \log[b_i(O_1)], \tag{B7}$$

and step through the observation sequence with

$$\phi_t(j) = \max_{1 \le i \le n} \left[\phi_{t-1}(i) + \log\, a_{ij}\right] + \log\left[b_j(O_t)\right]. \tag{B8}$$

[49] We terminate with

$$\log \boldsymbol{\mathcal{L}}^* = \max_{1 \le i \le n} [\phi_T(i)], \tag{B9}$$

which is the log likelihood of the best state sequence and the observations given the model. The backtracking step to recover the best state sequence is identical except that δ is replaced by ϕ in equations (equations (20)–(21)).

[50] **Acknowledgments.** I would like to thank Yariv Ephraim for pointing out the *Levinson* [1986] reference in the communication theory literature that allowed me to generate the reestimation equations for the Gamma density parameters in the hidden Markov models and Andy Solow for helpful discussions. The manuscript was improved by reviews from William Wilcock and an anonymous reviewer. This work was supported by the National Science Foundation (OCE-0137329).

References

Abromovitz, M., and I. A. Stegun (Eds.) (1965), *Handbook of Mathematical Functions*, Dover, New York.

Akaike, H. (1974), A new look at the statistical identification model, *IEEE Trans. Auto. Control*, *19*, 716–723.

Baum, L. E., and J. A. Eagon (1967), An inequality with applications to statistical estimation for probabilistic functions of Markov processes and to a model for ecology, *Bull. Am. Math. Soc.*, *73*, 360–363.

Baum, L. E., and T. Petrie (1966), Statistical inference for probabilistic functions of finite state Markov chains, *Ann. Math. Stat.*, *37*, 1554–1563.

Bremaud, P. (1998), *Markov Chains: Gibbs Fields, Monte Carlo Simulation, and Queues*, 444 pp., Springer, New York.

Crone, T. J., and W. S. D. Wilcock (2005), Modeling the effects of tidal loading on mid-ocean ridge hydrothermal systems, *Geochem. Geophys. Geosyst.*, *6*, Q07001, doi:10.1029/2004GC000905.

Davis, E., K. Becker, R. Dziak, J. Cassidy, K. Wang, and M. Lilley (2004), Hydrological response to a seafloor spreading episode on the Juan de Fuca ridge, *Nature*, *430*, 335–338.

deMartin, B. J., R. A. Sohn, J. P. Canales, and S. E. Humphris (2007), Kinematics and geometry of active detachment faulting beneath the Trans-Atlantic Geotraverse (TAG) hydrothermal field on the Mid-Atlantic Ridge, *Geology*, *35*, 711–714.

Dempster, A. P., N. M. Laird, and D. B. Rubin (1977), Maximum likelihood from incomplete data via the EM algorithm, *J. R. Stat. Soc., Ser. B*, *39*, 1–38.

Dziak, R. P., W. W. Chadwick Jr., C. G. Fox, and R. W. Embley (2003), Hydrothermal temperature changes at the southern Juan de Fuca Ridge associated with M_w 6.2 Blanco Transform earthquake, *Geology*, *31*, 119–122.

Ephraim, Y. (2002), Hidden Markov processes, *IEEE Trans. Inf. Theory*, *48*, 1518–1569.

Fornari, D., C. L. Van Dover, T. Shank, R. Lutz, and M. Olsson (1994), A versatile, low-cost temperature sensing device for time-series measurements at deep sea hydrothermal vents, *BRIDGE Newsl.*, *6*, 37–40.

Johnson, H. P., M. Hutnak, R. P. Dziak, C. G. Fox, I. Urcuyo, J. P. Cowen, J. Nabelek, and C. Fisher (2000), Earthquake-induced changes in a hydrothermal system on the Juan de Fuca mid-ocean ridge, *Nature*, *407*, 174–177.

Larson, B. I., E. J. Olson, and M. D. Lilley (2007), In situ measurement of dissolved chloride in high temperature hydrothermal fluids, *Geochim. Cosmochim. Acta*, *71*, 2510–2523.

Levinson, S. E. (1986), Continuously variable duration hidden Markov models for automatic speech recognition, *Comput. Speech Lang.*, *1*, 29–45.

Levinson, S. E., L. Rabiner, and M. Sondhi (1983), An introduction to the application of the theory of probabilistic functions of a Markov process to automatic speech recognition, *Bell Syst. Tech. J.*, *62*, 1035–1074.

Little, S. A., K. D. Stolzenbach, and F. J. Grassle (1988), Tidal Current Effects on Temperature in Diffuse Hydrothermal Flow: Guaymas Basin, *Geophys. Res. Lett.*, *15*, 1491–1494.

MacKay, R. J. (2002), Estimating the order of a hidden Markov model, *Can. J. Stat.*, *30*, 573–589.

Rabiner, L. R. (1989), A tutorial on hidden Markov models and selected applications in speech recognition, *Proc. IEEE*, *77*, 257–286.

Reves-Sohn, R., R. Thomson, and A. Rabinovich (2006), Tidal Dynamics in the Axial Valley of the Mid-Atlantic Ridge, *Eos Trans. AGU*, *87*, Fall Meet. Suppl., Abstract B31B-1101.

Robert, C. P., T. Ryden, and D. M. Titterington (2000), Bayesian inference in hidden Markov models through the reversible jump Markov chain Monte Carlo method, *J. R. Stat. Soc., Ser. B*, *62*, 57–75.

Roman, C. N., and H. Singh (2007), A self consistent bathymetric mapping algorithm, *J. Field Robotics*, *24*, 26–51.

Rubin, Y. (2003), *Applied Stochastic Hydrogeology*, 391 pp., Oxford Univ. Press, New York.

Ryden, T. (1995), Estimating the order of hidden Markov models, *Statistics*, *26*, 345–354.

Ryden, T., T. Teräsvirta, and S. Åsbrink (1998), Stylized facts of daily return series and the hidden Markov model, *Appl. Economet.*, *13*, 217–244.

Scheirer, D. S., T. M. Shank, and D. J. Fornari (2006), Temperature variations at diffuse and focused flow hydrothermal vent sites along the northern East Pacific Rise, *Geochem. Geophys. Geosyst.*, *7*, Q03002, doi:10.1029/2005GC001094.

Schwarz, G. (1978), Estimating the dimension of a model, *Anna. Stat.*, *6*, 461–464.

Sohn, R. A. (2007), Stochastic analysis of exit fluid temperature records from the active TAG hydrothermal mound (Mid-Atlantic Ridge, 26°N): 1. Modes of variability and implications for subsurface flow, *J. Geophys. Res.*, *112*, B07101, doi:10.1029/2006JB004435.

Sohn, R. A., D. J. Fornari, K. L. von Damm, J. A. Hildebrand, and C. S. Webb (1998), Seismic and hydrothermal evidence for a cracking event on the East Pacific Rise crest at 9°50′N, *Nature*, *396*, 159–161.

Tivey, M. K., A. M. Bradley, T. M. Joyce, and D. Kadko (2002), Insights into tide-related variability at seafloor hydrothermal vents from time-series temperature measurements, *Earth Planet. Sci. Lett.*, *202*, 693–707.

Viterbi, A. J. (1967), Error bounds for convolutional codes and an asymptotically optimum decoding algorithm, *IEEE Trans. Inf. Theory*, *IT-13*, 260–269.

Wilcock, W. S. D. (2004), Physical response of mid-ocean ridge hydrothermal systems to local earthquakes, *Geochem. Geophys. Geosyst.*, *5*, Q11009, doi:10.1029/2004GC000701.

Wilcock, W. S. D., S. D. Archer, and G. M. Purdy (2002), Microearthquakes on the Endeavour segment of the Juan de Fuca Ridge, *J. Geophys. Res.*, *107*(B12), 2336, doi:10.1029/2001JB000505.

R. A. Sohn, Woods Hole Oceanographic Institution, Woods Hole, MA 02543, USA. (rsohn@whoi.edu)